# INVESTIGATING THE CORROSION BEHAVIOR OF NANO STRUCTURED COPPER STRIP PRODUCED BY ACCUMULATIVE ROLL BONDING (ARB) PROCESS IN ACIDIC CHLORIDE ENVIRONMENT

**A. Nikfahm[1,*], I. Danaee[1] , A. Ashrafi[2] and M. R. Toroghinejad[3]**

* *Nikfahm2012@gmail.com*

**Received: March 2013** **Accepted: October 2013**

**[1] Department of Technical Inspection Engineering, Abadan Faculty of Petroleum Engineering, Petroleum University of Technology, Abadan, Iran.**

**[2] Department of Materials Engineering, Faculty of Engineering, Shahid Chamran University, Ahvaz, Iran.**

**[3] Department of Materials Engineering, Isfahan University of Technology, Isfahan, Iran.**

***Abstract:*** *In this research accumulative roll bonding process as sever plastic deformation process was applied up to 8 cycles to produce the ultrafine grain copper. Microstructure of cycle 1, cycle 4 and cycle 8 investigated by TEM images. By analyzing TEM images the grain size measured below 100 nm in cycle 8 and it was with an average grain size of 200 nm. Corrosion resistance of rolled copper strips in comparing with unrolled copper strip was investigated in acidic (pH=2) 3.5 wt. % NaCl solution. Potentiodynamic polarization and EIS tests used for corrosion resistance investigations. The corrosion morphologies analyzed by FE-SEM microscopy after polarization test and immersion for 40 hours. Results show that the corrosion resistance decreased up to cycle 2 and increased after rolled for forth time. The corrosion degradation was more intergranular in cycle 2 and unrolled counterpart. It was more uniform rather than intergranular type in cycle 8. Corrosion current density in unrolled sample (2.55 $\mu Acm^{-2}$) was about two times of that in cycle 8 (1.45 $\mu Acm^{-2}$). The higher corrosion rate in cycle 2 in comparison with others was attributed to unstable microstructure and increase in dislocation density whereas the uniform corrosion in cycle 8 was due to stable UFG formation.*

***Keywords:*** *Ultrafine Grain, Corrosion, Copper, NaCl, Accumulative Roll Bonding, SPD*

## 1. INTRODUCTION

During the last decade a variety of techniques for fabrication of ultra-fine grained (UFG) materials with nanocrystalline or sub-microcrystalline structure were developed [1, 2]. Severe Plastic Deformation (SPD) can be explained as deformation to large strains below recrystallization temperature without intermediate thermal treatments that can result in UFG structures [3]. The accumulative roll bonding (ARB) is one of the severe plastic deformations that proposed by Saito et al. [4]. The advantage of this process is its applicability to large bulky and sheet materials [5-7] and is a continuous process.

Copper and copper alloys are widely used as condenser and heat exchanger tubing materials, in plate heat exchangers and as one of radioactive waste container metals and in other industries due to its high thermal conductivity, good corrosion resistance, and mechanical workability. New industrial challenges require the production of improved high strength/ductile materials, reflected by the research for over two decades on nano structured copper. These materials can be used in industries that heat transferring properties and strength of them are important due to their application. However, for nano structured or submicron copper to be widely used, it is necessary to study its mechanical and physical properties in detail, such as corrosion resistance [8]. The corrosion behaviour of nanostructured copper produced by SPD methods has been only less considered. Vinogradov et al. [9] have first reported the anodic polarization behaviour of UFG copper fabricated by Equal-channel angular pressing (ECAP) in modified Livingstone etchant, and concluded that the anodic current in UFG copper is higher in both active and passive regions than that of coarse grained (CG) counterparts. However, the

**Table 1.** Specification of initial copper strip.

| Material | Chemical composition |
|---|---|
| Tough pitch copper | Cu 99.9% (mass), Oxygen ~250 ppm, Other impurities ~less than 20 ppm |

corroded surface appeared rather smooth with shallow corrosion grooves at the grain boundaries whereas deeper grooves were formed at the grain boundaries in CG copper. Zheng et al. showed that the corrosion current of ECAPed copper in Hanks solution is higher than that of the coarse grained copper [10]. Hashimoto et al. investigated the stress-corrosion cracking (SCC) of ultra-fine grain copper produced by ECAP method in 1 M $NaNO_2$ aqueous solution. They found that UFG copper possesses notably better resistance to SCC when compared to its coarse-grain counterpart [11]. Miyamoto et al. reported that UFG copper exhibited a lower corrosion current in comparison with that in its recrystallized coarse grain (CG) counterpart in Livingstone etchant [12]. The unaffected general corrosion characteristics and homogeneous damage in UFG copper in 3 % NaCl, 1M HCl and the standard Livingston solution was reported by Milos and et al. [13]. The evaluation of corrosion behavior of sheets rolled by ARB process as a SPD method has been only less considered up to now [14-17] and there are different results in corrosion properties of that nano structured materials which produced with SPD methods as mentioned above. So, it is not correct to attribute the lower or higher corrosion resistance to UFG materials in this case to copper and due to different corrosion behavior of UFG copper in different studied environments, it is necessary to investigation of corrosion behavior of copper in any specific method of fabrication. The aim of this study is to evaluate the corrosion behavior of pure copper strip fabricated by ARB process in acidic NaCl aqueous solution at ambient temperature.

## 2. EXPERIMENTAL PROCEDURE

### 2.1. Specimen Preparation

The material used in this study was tough pitch copper (99.9%). The dimensions of initial sheets were 1 mm in thickness, 30 mm wide and 300 mm long. One side of the surface of the sheets was degreased by acetone and wire-brushed. After the surface treatment, two pieces of the sheets were stacked so that the brushed surfaces were in contact and were fixed to each other tightly by copper wires and then rolled. The roll diameter was 127 mm and the rolling speed was about 6 m/min. In the present study, the ARB process up to 8 cycles was performed at ambient temperature without lubrication. The sheets were air-cooled after roll bonding.

The microstructural evaluations were done by PHILIPS CM200 transmission electron microscopy (TEM) for the specimens after ARB. Thin foils parallel to the rolling plane were prepared so that the observed position was about 300 μm below surface. Selected area diffraction (SAD) patterns also were taken. Samples with dimensions of 7 mm * 15 mm (Area ≈ 1$cm^2$) prepared from the rolled copper sheets and covered by epoxy resin leaving only the 1$cm^2$ surface for corrosion tests. The samples of cycle no. 1, 2, 4, 6 and 8 used for the comparing the corrosion behavior with unrolled copper strip. The chemical compositions of tough pitch copper have been shown in Table 1.

### 2. 2. Corrosion Experiments

Electrochemical experiments were performed using a three electrode cell at T= 25±1 °C, in 3.5 wt. % NaCl aqueous solution with pH=2. PH of the solutions was adjusted by HCl. A platinum plate and a saturated calomel electrode (SCE) were served as counter and reference electrode, respectively. The potentiodynamic polarization and electrochemical impedance spectroscopy (EIS) tests performed on an AutoLab PGSTAT302N potentiostat system. The polarization test was carried out at the scanning rate of 1 mV/s from -0.45 V bellow the OCP up

to 0.35 V above the OCP. The frequency range in the EIS test was from 100 kIIz to 10 mIIz using voltage amplitude of 10 mV. Before each test, the samples were immersed in the electrolyte for 20 min to stabilize the open circuit potential. The morphologies of the corroded surfaces after polarization tests were examined using FE-SEM HITACHI S-4160 scanning electron microscopy for samples of cycle 2, 8 and unrolled one. Also the microscope was used to analysis of corroded surface after immersion.

## 3. RESULTS AND DISCUSSION

### 3. 1. Microstructure

Fig. 1 shows the TEM microstructures and corresponding SAD patterns observed at rolling plane of ARB specimens produced by 1, 4 and 8 cycles. After 1 cycle of the ARB process the microstructure showed a mixture of non-deformed and deformed grains with some dislocation tangles (Fig. 1a). It is not surprising because plastic deformation is inherently an inhomogeneous process. The SAD pattern of this sample was taken from a single crystal that shows no deformation has occurred in this grain. For the specimen after 4 cycles, the dislocation density increased and cell structures were observed. Also the microstructure became more uniform and some grains with an average grain size of 200 nm have formed. The SAD patterns of the 4 cycles ARB sample is more diffused than that of the single cycle sample and gradually evolves into ring pattern consisting of discrete spots (Fig. 1b). This may indicates that examined area has subdivided into small domains with wide orientation spread. With increasing the strain up to 8 cycles, the dislocation density at grain interior seemed lower than those after 4 ARB cycles. It is noteworthy that small recrystallized grains were observed along with the ultrafine deformation microstructures, as seen in Fig. 1c. The average grain size of these equiaxed recrystallized grains is below 100 nm, smaller than that after 4 cycles. The mean grain size of pure copper fabricated by ARB process has been reported about 260 – 300 nm by other researchers [6, 18, 19].

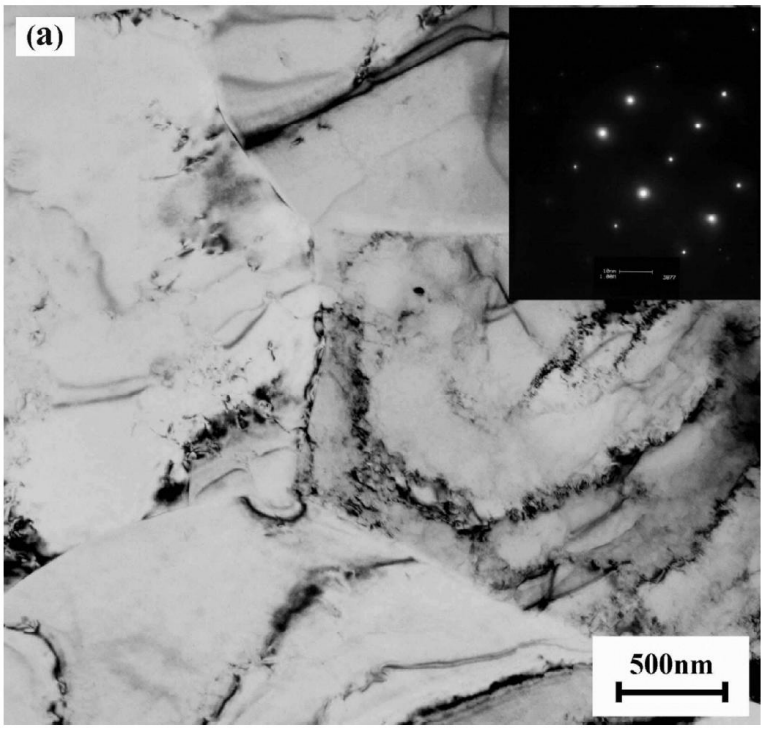

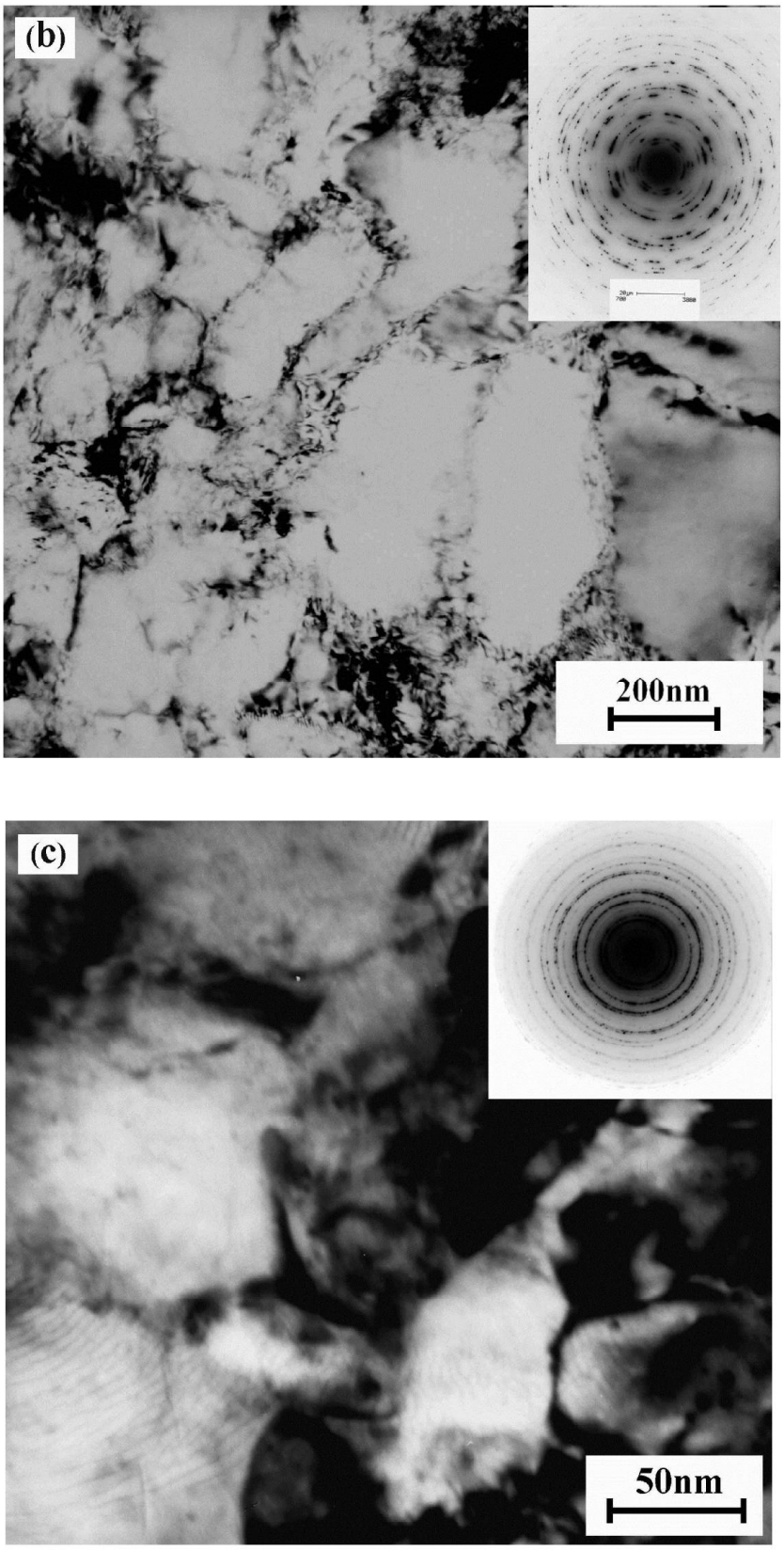


**Fig. 1.** Typical TEM micrographs and the matching SAD patterns from RD–TD planes of ARB processed copper by (a) 1 cycle, (b) 4 cycle and (c) 8 cycle

### 3. 2. Polarization Results

The potentiodynamic polarization curves for accumulative roll bonded (ARBed) copper in comparison with coarse grain (CG) Cu in 3.5 wt. % NaCl with pH=2 is shown in Fig. 2.

The general shape of polarization curves for ARBed samples do not change substantially with that of CG sample in this acidic chloride environment, reflecting similar dissolution behaviors of samples. All copper samples display an active-passive-transpassive behavior. In anodic region of polarization plots the increasing in current density is related to dissolution of copper to the cupric ions which finally the current density reaches to maximum amount, after that the formation of CuCl started and the current decreased to its minimum amount due to surface coverage with CuCl layer. The current due to instability of CuCl compound and reaction of $Cl^-$ with CuCl increased which leads to formation of soluble $CuCl^-_2$ and the corrosion process goes

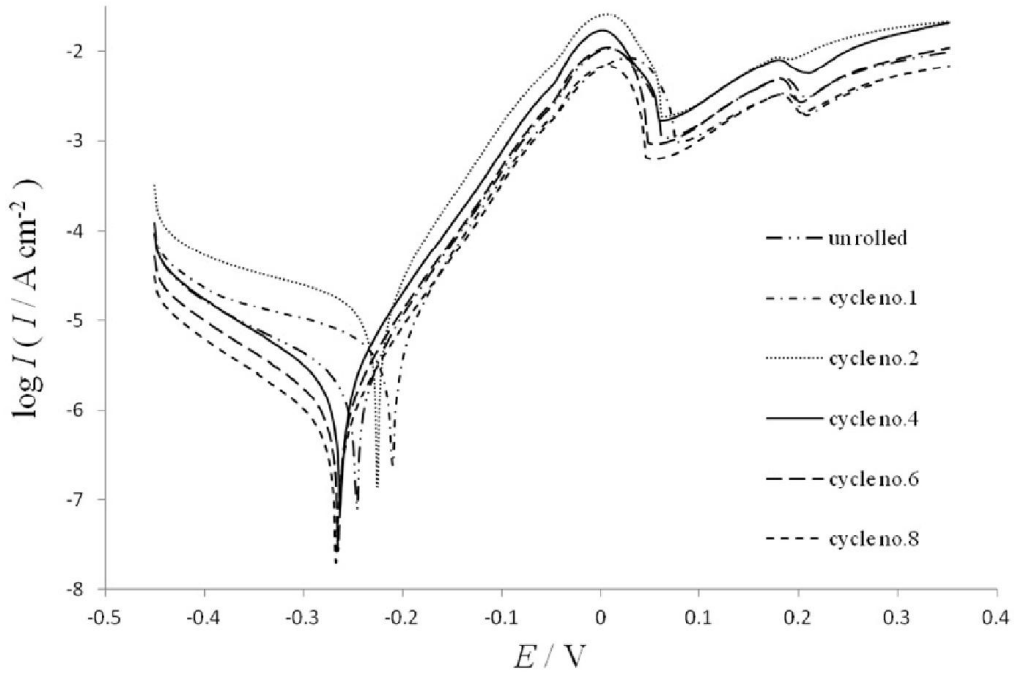


**Fig. 2.** Polarization curves of unrolled and ARBed copper samples in 3.5 wt. % NaCl with pH=2 at 25±1°C.

**Table 2.** corrosion parameters for unrolled and ARBed copper samples in 3.5 % NaCl pH=2 at 25±1°C.

| Sample | $i_{corr}$/μAcm$^{-2}$ | -$E_{corr}$(v) | $\beta_c$/mvdec$^{-1}$ | $\beta_a$/mvdec$^{-1}$ | CR (mm.year$^{-1}$) |
|---|---|---|---|---|---|
| **Unrolled** | *2.55* | *0.246* | *0.198* | *0.066* | *5.913E-2* |
| **Cycle no.1** | *2.80* | *0.210* | *0.243* | *0.067* | *6.493E-2* |
| **Cycle no.2** | *3.37* | *0.220* | *0.204* | *0.066* | *7.815E-2* |
| **Cycle no.4** | *2.68* | *0.257* | *0.228* | *0.066* | *6.215E-2* |
| **Cycle no.6** | *1.67* | *0.264* | *0.196* | *0.066* | *3.872E-2* |
| **Cycle no.8** | *1.45* | *0.267* | *0.162* | *0.066* | *3.362E-2* |

back in potentials vicinity of 0.2 V. Diffusion of $CuCl^-_2$ to solution controlled the corrosion. The peaks on the polarization curves are related to formation of these compounds the details of reactions has been discussed elsewhere [20].

The Tafel extrapolation method was used to evaluate the corrosion parameters. The results for corrosion current densities ($i_{corr}$) and other parameters are summarized in Table 2 and Fig. 3. The highest corrosion current obtained for cycle 2 and the minimum amount was for cycle 8. As it can be seen in table 2, after cycle 4 corrosion current has been lowered whereas the current was ascending until cycle 2, these all variations attributed to the microstructure of samples that has been changed through ARB process. This reduction in tendency to being active after cycle 4 is related to the microstructure stability.

As shown in the TEM images of cycle 1, 4, and 8 the dislocation density increased with application of ARB process. After cycle 4 the cells have been formed and UFG grains have been formed in cycle 8 which the UFG size in cycle 8 was bellow 100 nm. Generally with application of cold work on metals, due to some plastic deformations external energy induced to the metal and the structure becomes unstable. With respect to the results of corrosion behavior investigation and microstructure analysis, it concluded that the stability in upper cycles was due to UFG formation. The highest corrosion current in cycle 2 has been confirmed microstructure instability of this sample.

From the polarization plots in Fig. 2, it was clear that in a specific cathodic potential for example in E= -0.4 V the cathodic current density for cycle 8 was lower than that of cycle 6 and 4. So the lower corrosion current in upper cycles can be the interaction in cathodic reactions. The grain size of copper reached to bellow 100 nm in cycle 8 with ARB process. The grain interiors are the cathodic sites and the grain boundaries due to their lower potential in comparing with grain interiors are the anodic sites. The reduction of cathodic sites (grain interior) to nano scale leads to restriction in the corrosion process due to cathodic control in other words the cupric ions flow and covers the grain interior and interacted in the reduction reactions, therefore the anodic reaction stopped. Miyamoto et al. [12] reported one of the reasons of reduction in corrosion current of ECAPed copper, the interaction in cathodic reaction in this way that explained. It concluded that the variation in corrosion currents

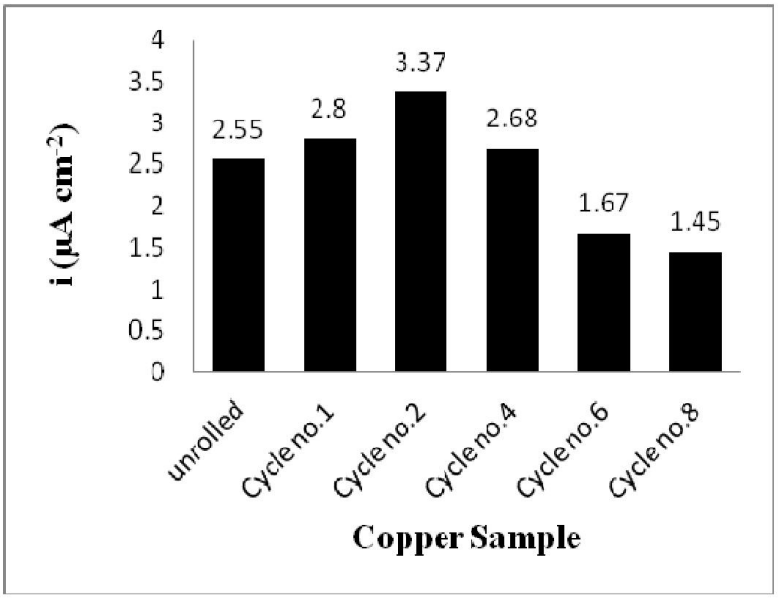


**Fig. 3.** corrosion current density of unrolled and ARBed copper samples

in this work was due to the effect of kinetic of reactions.

In Fig. 2, it can be seen that the critical current for (CuCl) formation in cycle 2 was higher than its amount for other samples. This is due to existence of more anodic and active sites in cycle 2 and refers to the unstable microstructure of this sample in comparison to others which leads to higher kinetics of anodic reactions.

### 3. 3. EIS Results

Fig. 4 shows the typical Nyquist plots obtained for the different copper samples at an open-circuit potential after 20 min immersion in 3.5% NaCl with pH=2. Fitting of experimental impedance spectroscopy data to the proposed equivalent circuit was done by means of home written least square software based on the Marquardt method for the optimization of functions and Macdonald weighting for the real and imaginary parts of the impedance [21, 22]. The equivalent circuit has been shown in Fig. 5. The depressed semicircle in the high frequency can be related to the charge transfer resistance and the double-layer capacitance. To obtain a satisfactory impedance simulation of copper, it is necessary to replace the capacitor ($C$) with a constant phase element ($CPE$) $Q$ in the equivalent circuit [23]. The most widely accepted explanation for the presence of $CPE$ behavior and depressed semicircles on solid electrodes is microscopic roughness, causing an inhomogeneous distribution in the solution resistance as well as in the double-layer capacitance [24]. The impedance of the $CPE$ is defined as $Z_{CPE}=1/Q(iw)^n$, where $Q$ is a capacitive parameter related to the average double layer capacitance ($C_{dl}$), and $n$ is a dimensionless parameter related to the constant phase angle. In equivalent electrical circuit, $R_s$, $CPE_{dl}$, $R_{ct}$ and $W$ represent solution resistance, a constant phase element corresponding to the double layer capacitance, the charge transfer resistance and the Warburg impedance. This electrochemical circuit fitted acceptably on the EIS spectra with mean square error less than 0.05. Table 3 illustrates the equivalent circuit parameters for the impedance spectra of copper samples in acidic NaCl solution. The presence of Warburg impedance in lower frequencies shows that the corrosion is controlled by diffusion of products or aggressive ions through the corrosion product on the surface to/from the solution. Therefore

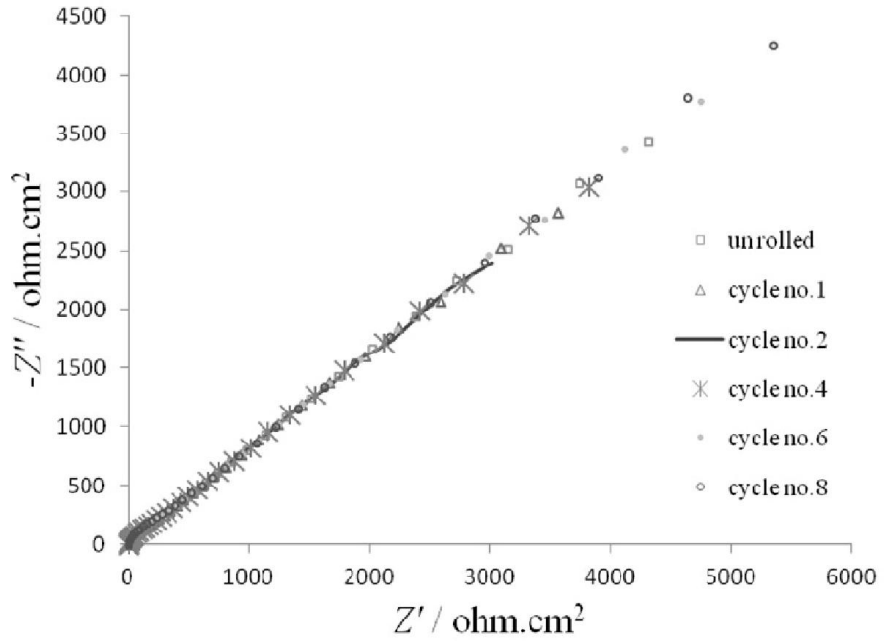


**Fig. 4.** Typical Nyquist impedance plots for ARBed and unrolled copper samples in 3.5%NaCl at 25±1°C with pH=2

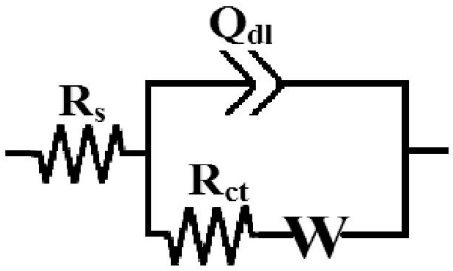


**Fig. 5.** Equivalent circuit used to model impedance data for ARBed and unrolled copper samples in 3.5% NaCl solution with pH=2 at 25 ±1C.

diffusion of Cl- from the solution to the interface and reaction with the CuCl layer and finally diffusion of soluble $CuCl_2$- to the solution have been controlled the corrosion rate [25].

### 3. 4. Morphology of Corroded Surfaces after Immersion

For precise investigations of corrosion behavior of the ARBed copper samples in acidic sodium chloride media, the ARBed samples of cycle no.1,2,4 and 8 immersed in 3.5 wt. % NaCl with pH=2, for 40 hours.

The view of corroded surfaces of ARBed cycle no.1, 2, 4 and 8 samples after natural immersions has been shown in Fig. 6.

As seen, the corroded surfaces covered with corrosion products. The products in this environment are CuCl that are unstable and insoluble which its reactions with $Cl^-$ lead to corrosion of copper [20]. Differences between the appearances of corroded surfaces have been seen. The size of products seems be compact and smaller in cycle No.4 and 8 and its reason is the finer microstructure of these samples in comparing with cycle no.1 and 2. The large corrosion products in cycle no.1 have clearly been seen. The grains in cycle No.1 deformed heterogeneity and many of them were intact, for this reason the corroded surface of this sample are seen coarser than others.

In cycle 2 many of grains deformed but the bulk and finally the surface of this sample are disorder than others because of accumulation of dislocation locally and nonentity of new grain formation. Because of cell formation in cycle no.4 as mentioned in TEM results the corroded surface was homogenous than lower cycles, so the corrosion products on surface of cycle no.4 are more compact than that of cycle No.2. The corrosion products on surface of sample cycle 8 were smooth and uniform than others, also the products seam more compact. The surface in cycle 4 and 8 covered more than others so the corrosion products on surface of these samples

**Table 3.** Electrochemical parameters calculated from EIS measurements on copper electrode in 3.5%NaCl solution with pH= 2, at 25 ±1°C using equivalent circuit presented in Fig.5.

| Sample | $R_s$ / Ω cm$^2$ | $Q_{dl}$ / F | $N$ | $R_{ct}$ / Ω cm$^2$ | $W$ / Ω$^{-1}$ cm$^{-2}$ s$^{1/2}$ |
|---|---|---|---|---|---|
| **Unrolled** | *3.393* | $4.76\times10^{-5}$ | *0.86* | *251.2* | $6.74\times10^{-4}$ |
| **Cycle no.1** | *2.734* | $5.77\times10^{-5}$ | *0.87* | *207.2* | $8.17\times10^{-4}$ |
| **Cycle no.2** | *2.158* | $6.81\times10^{-5}$ | *0.86* | *175.8* | $9.64\times10^{-4}$ |
| **Cycle no.4** | *2.545* | $5.37\times10^{-5}$ | *0.86* | *222.6* | $7.61\times10^{-4}$ |
| **Cycle no.6** | *3.084* | $4.33\times10^{-5}$ | *0.87* | *276.2* | $6.13\times10^{-4}$ |
| **Cycle no.8** | *3.821* | $3.84\times10^{-5}$ | *0.86* | *311.2* | $5.44\times10^{-4}$ |

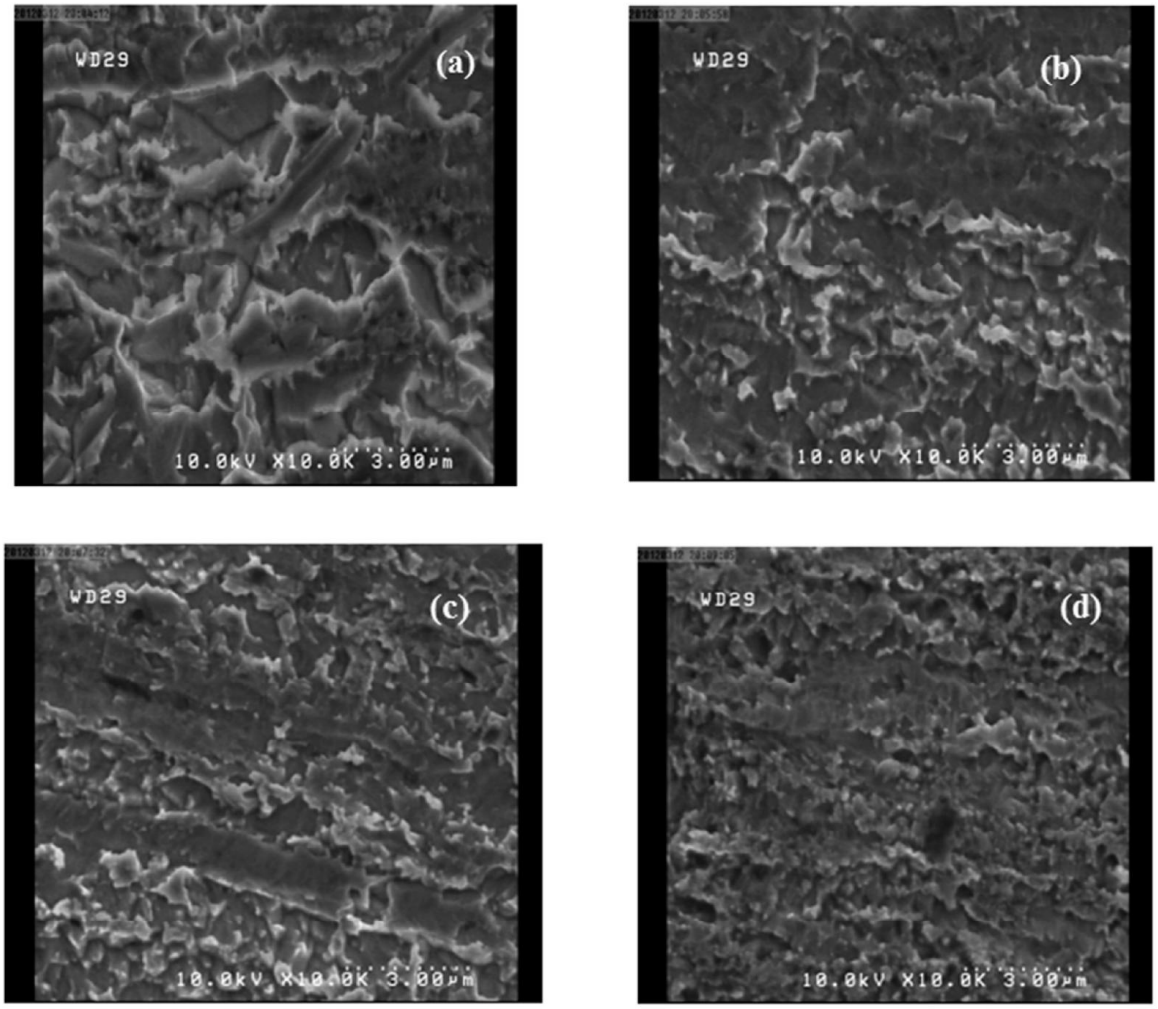


**Fig. 6.** FE-SEM images of corroded surfaces of ARBed copper samples after immersion in 3.5 wt. % NaCl at 25±1°C with pH=2 (a): cycle no.1, (b): cycle no.2, (c): cycle no.4, (d): cycle no.8.

can be impenetrable in comparing with others.

### 3. 5. Morphology of Corroded Surface After Polarization

Localized degradation is known as a decisive factor in environmentally assisted fracture. Hence, to characterize the overall resistance against environmental attack it is necessary to evaluate the degree of localization of corrosion damage.

From a metallurgical viewpoint, corrosion is particularly associated with structural heterogeneity resulting from precipitations and other lattice defects. One of the most dangerous localized damage is intergranular corrosion associated with grain boundaries [13].

So for precise investigation of grain boundary corrosion after polarization the morphologies investigated by FE-SEM pictures. Due to lower corrosion rate and UFG formation in cycle 8 it is important to investigate the grain boundary attack in this sample in comparing to lower cycles for some applications.

Fig. 7 shows the surface morphologies of samples after potentiodynamic polarization test. The finer microstructure is to fracture of some grains to new small grains during the process in comparing unrolled one which larger grains seen.

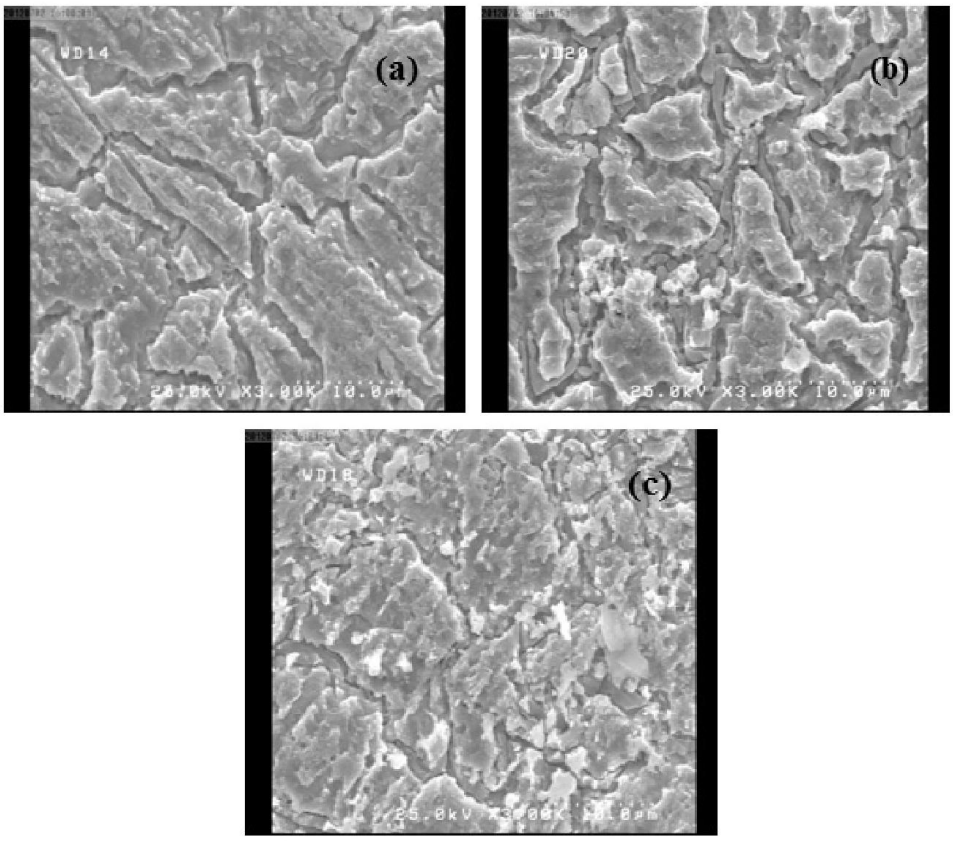


**Fig.7.** FE-SEM images of corroded surfaces after polarization in 3.5 wt. % NaCl at 25±1°C with pH=2 (a): unrolled, (b): cycle no.2, (c): cycle no.8.

The grain boundary attacks are visible clearly in unrolled sample and cycle no.2. As seen the corroded grain boundaries are narrow in unrolled sample in comparing to cycle no.2 and the volume fraction of them is lower than that of cycle 2 but because of dislocation accumulation in grain boundaries of cycle 2, the boundaries attacked more and grooves have been broader than unrolled material. The corroded surface of cycle 2 was coarser than unrolled sample. The polarized surface of cycle no.8 seems to be smooth than unrolled and sample of cycle 2. seen in cycle no.2 due As mentioned the dislocation density increased with ARB process until the dislocations lead to the formation of new cells and UFG grains uniformly in cycle 8. When aggressive ions attack to this surface, as shown it corroded uniformly than lower cycles because the potential difference in entire surface is very low. As seen in the surface of cycle 8 the grain boundaries has not been attacked that it is attributed to the high activity of entire surface atoms which distribute homogeneity so the corrosion products covered homogeneity the surface. As seen the UFGs in this cycle has an important role in changing the type of corrosion.

## 4. CONCLUSION

The following conclusions are drawn from this research:

TEM analysis show that after 4 cycles ARB process grains with an average grain size of 200 nm have formed and the grain size was below 100 nm in cycle 8. The corrosion rate increased until cycle 2 with ARB process and decreased after rolled for fourth time. The general shape of the polarization and Nyquist plots was very similar for all samples in the experiment environment, indicating that almost no change in the corrosion mechanism occurred due to the grain refinement and UFG formation. Corrosion

morphology images show that in upper cycles the corrosion products were compact and corroded surface seems smooth and uniform, but in lower cycles the corrosion degradation was more in intergranular region. Finally it concluded that the corrosion rate of unrolled copper sheet was about two times of that in cycle 8.

## ACKNOWLEDGEMENT

Appreciation is to Iranian Nano Technology Initiative Council for financially supporting of this work.

## REFERENCES

1. H. Gleiter, Materials with ultrafine microstructures, Retrospectives and perspectives, Nanostruct. Mater. 1992, 1, 1.
2. V. M. Segal, Materials processing by simple shear, Mater. Sci. Eng. A 1995, 197, 157.
3. B. Cherukuri, T. S. Nedkova, R. Srinivasan, A comparison of the properties of SPD-processed AA-6061 by equal-channel angular pressing, multi-axial compressions/forgings and accumulative roll bonding, Mater. Sci. Eng. A 2005, 410–411, 394.
4. Y. Saito, H. Utsunomiya, N. Tsuji, T. Sakai, Novel ultra-high straining process for bulk materials-development of the accumulative roll-bonding (ARB) process, Acta Mater. 1999, 47, 579.
5. X. Huang, N. Tsuji, Y. Minamino, N. Hansen, The 22nd Riso Inter. Symp. on Materials Science, Roskilde, Denmark, 2001, 255.
6. N. Tsuji, Y. Saito, S.H. Lee, Y. Minamino, ARB (Accumulative Roll-Bonding) and other new Techniques to Produce Bulk Ultrafine Grained Materials, Adv. Eng. Mater. 2003, 5, 338.
7. N. Tsuji, Y. Saito, H. Utsunomiya, S. Tanigawa, Ultra-fine grained bulk steel produced by accumulative roll-bonding (ARB) process, Scripta Mater. 1999, 40, 795.
8. P. M. Gordo, M. Duarte Naia, A.S. Ramos, M.T. Vieira, Zs. Kajcsos, "Positron studies on nanocrystalline copper thin films doped with nitrogen", in: ICPA15 – 15th International Conference on Positron Annihilation, Kolkata, India, 2009.
9. A. Vinogradov, T. Mimaki, S. Hashimoto, R.Z. Valiev, On the corrosion behaviour of ultra-fine grain copper, Scripta Mater. 1999, 41, 319–326.
10. X. X. Xu, F.L. Nie, J.X. Zhang, W. Zheng, Y.F. Zheng, C. Hu, G. Yang, Corrosion and ion release behavior of ultra-fine grained bulk pure copper fabricated by ECAP in Hanks solution as potential biomaterial for contraception, Mater. Lett. 2010, 64, 524–527.
11. T. Yamasaki, H. Miyamoto, T. Mimaki, A. Vinogradov , S. Hashimoto, Stress corrosion cracking susceptibility of ultra-fine grain copper produced by equal-channel angular pressing, Materials Science and Engineering A 2001, 318, 122–128.
12. H. Miyamoto, K. Harada, T. Mimaki, A. Vinogradov, S. Hashimoto, Corrosion of ultra-fine grained copper fabricated by equal-channel angular pressing, Corr. Sci. 2008, 50, 1215–1220.
13. M. Janeceki, B. Hadzima, R. J. Hellma, Y. Estrin, The influence of microstructure on the corrosion properties of Cu polycrystals prepared by ECAP, Kovove Mater. 2005, 43, 258-271.
14. E. Darmiani, I. Danaee,MA. Golozar and MR.Toroghinejad Corrosion investigation of Al-SiC nano-composite fabricated by accumulative roll bonding (ARB) process. Journal of Alloys and Compounds. 2013,552,31-39.
15. M. Kadkhodaee, M. Babaiee, HD. Manesh, M. Pakshir and B. Hashemi. Evaluation of corrosion properties of Al/nanosilica nanocomposite sheets produced by accumulative roll bonding (ARB) process. Journal of Alloys and Compounds. 2013,576,66-71.
16. W. Wei, Wei K. Xia and Du Q. Bo. Corrosion and tensile behaviors of ultra-fine grained Al-Mn alloy produced by accumulative roll bonding. Materials Science and Engineering: A. 2007,454-455,536-541.
17. MF. Naeini, MH. Shariat and M. Eizadjou. On the chloride-induced pitting of ultra fine grains 5052 aluminum alloy produced by accumulative roll bonding process. Journal of Alloys and Compounds. 2011,509,4696-4700.
18. Y. H. Jang, S.S. Kim, S.Z. Han, C.Y. Lim, C.J.

Kim, M. Goto, Effect of trace phosphorous on tensile behavior of accumulative roll bonded oxygen-free copper, Scripta Mater. 2005, 52, 21.

19. S. Z. Han, C. Lim, C.J. Kim, S. Kim, Mechanical properties of SPD (sever plastic deformation) processed copper, Mater. Sci. Forum , 2005, 475–479, 3497.
20. W. Li, L. Hu, Sh. Zhang, B. Hou, Effects of two fungicides on the corrosion resistance of copper in 3.5% NaCl solution under various conditions, Corr. Sci. 2011, 53, 735-745.
21. I. Danaee, J. Electroanal. Chem. 2011, 662,415-420.
22. J. R. Macdonald, Solid State Ion. 1984, 13,147-149.
23. I. Danaee, M. Niknejad Khomami and AA. Attar. Corrosion behavior of AISI 4130 steel alloy in ethylene glycol-water mixture in presence of molybdate. Materials Chemistry and Physics. 2012, 135,658-667.
24. I. Danaee and S. Noori, Kinetics of the hydrogen evolution reaction on NiMn graphite modified electrode.International Journal of Hydrogen Energy. 2011,36,12102-12111.
25. MM. Antonijevic, SC. Alagic, MB. Petrovic, MB. Radovanovic and AT. Stamenkovic. The Influence of pH on Electrochemical Behavior of Copper in Presence of Chloride Ions. International Journal of Electrochemical Science.2009,4,516-524.